

Propagation of terahertz pulses in random media

BY JEREMY PEARCE, ZHONGPING JIAN AND DANIEL M. MITTLEMAN

*Department of Electrical and Computer Engineering, Rice University,
MS 366, Houston, TX 77251-1892, USA (daniel@rice.edu)*

Published online 16 December 2003

We describe measurements of single-cycle terahertz pulse propagation in a random medium. The unique capabilities of terahertz time-domain spectroscopy permit the characterization of a multiply scattered field with unprecedented spatial and temporal resolution. With these results, we can develop a framework for understanding the statistics of broadband laser speckle. Also, the ability to extract information on the phase of the field opens up new possibilities for characterizing multiply scattered waves. We illustrate this with a simple example, which involves computing a time-windowed temporal correlation between fields measured at different spatial locations. This enables the identification of individual scattering events, and could lead to a new method for imaging in random media.

Keywords: terahertz imaging; photon diffusion; random media; multiple scattering

1. Introduction

Measurements of diffuse photons have proven to be a powerful tool in statistical optics. Narrowband diffuse photon density waves can be used for imaging of objects immersed in a random medium (Lasocki *et al.* 1998; O'Leary *et al.* 1995; Ripoll & Nieto-Vesperinas 1999; Schotland & Markel 2001). It is also possible to extract information using diffusing wave spectroscopy, which involves measurements of the temporal intensity or field correlations in a dynamic random medium (Boas & Yodh 1997; Boas *et al.* 1995; Pine *et al.* 1988). Alternatively, one can obtain similar data from spatial correlations within a speckle pattern (Berkovits & Feng 1990; Naulleau *et al.* 1995; Thompson *et al.* 1997). All of these techniques have found broad applicability, particularly in the field of biomedical imaging. However, due to the difficulties associated with determining the phase of an optical field, all rely on measurements of light intensity, rather than electric field. Furthermore, intensities are generally measured only in an average sense, over a time-scale much longer than the optical period. A notable exception involves time-resolved field measurements using microwave techniques (Genack *et al.* 1999; Sebbah *et al.* 2000; van Tiggelen *et al.* 1999). However, these have generally employed a waveguide geometry in which the issue of imaging does not generally arise.

One contribution of 16 to a Discussion Meeting 'The terahertz gap: the generation of far-infrared radiation and its applications'.

In this work, we describe measurements of photon diffusion using terahertz time-domain spectroscopy (THz TDS). This technique permits us to characterize both the amplitude and phase variations of a random electromagnetic field with a spatial resolution smaller than the size of a speckle spot and a temporal resolution better than one optical cycle. As a first step, it is necessary to characterize the statistics of the diffusive component of the wave. These statistics can be used to extract information on the nature of the random medium (Thompson *et al.* 1997), and are a key indicator of the onset of localization (Rivas *et al.* 2001). We then explore the computation of temporal correlations between fields measured at different spatial locations. We demonstrate that this permits us to obtain information about *individual scattering events* experienced by portions of the diffusing field, and holds great promise for the location and characterization of objects buried within the random medium.

2. Statistics of broadband diffusive pulses

Much of the research on diffusive optical waves has concentrated on the case of monochromatic or narrowband waves (Boas *et al.* 1995; Feng *et al.* 1988; Genack *et al.* 1990, 1999; Matson 1997; O’Leary *et al.* 1992; Sebbah *et al.* 2000; Webster *et al.* 2002). Several authors have used short optical pulses as a means of separating the diffusive portion of the wave from the ballistic light (Bashkansky *et al.* 1994; Herrmann *et al.* 2002; Rivas *et al.* 2001; Yoo *et al.* 1991, 1992). Others have used low-coherence interferometry to extract relative phase information (Brodsky *et al.* 1997, 2000; Petoukhova *et al.* 2001; Popescu & Dogariu 1999; Thurber *et al.* 2000). However, the treatment of the statistics of broadband fields in random media have not been addressed.

Here, we report measurements of the electric field of multiply scattered broadband optical pulses (Pearce *et al.* 2003). We compute the statistics of these random fields and demonstrate the connections to the case of monochromatic radiation. These measurements employ THz TDS, in a configuration quite similar to the one described previously (Mittleman *et al.* 1996, 1999). Using this technique, it is possible to generate pulses with a fractional bandwidth in excess of 100% (50 GHz–1 THz). Furthermore, the coherent measurement of the electric field permits extraction of both the amplitude and phase of the field, with a temporal resolution better than one optical cycle, without the use of interferometric techniques. As a result, one directly observes, among other things, the distribution of photon transit times (i.e. the time-of-flight distribution function). This quantity usually must be extracted from time-integrated measurements using spatial intensity correlations (Webster *et al.* 2002). Finally, we emphasize that these measurements have been performed in a three-dimensional sample, rather than in the waveguide geometry customarily employed in microwave measurements (Chabanov & Genack 1997).

The experimental set-up is illustrated in figure 1. Single-cycle terahertz pulses are focused into a random medium, and the emerging radiation is measured at an angle θ with respect to the transmitted beam direction. In these initial measurements, the angle is fixed at $\theta = 90^\circ$. This set-up ensures that no ballistic radiation reaches the detector. The model random medium consists of a large number of teflon spheres with a diameter of 0.794 ± 0.025 mm, contained in a cell with teflon walls. Teflon is an excellent material for these measurements, because of its low absorption and because the refractive index of teflon, $n = 1.4330$, is nearly independent of frequency

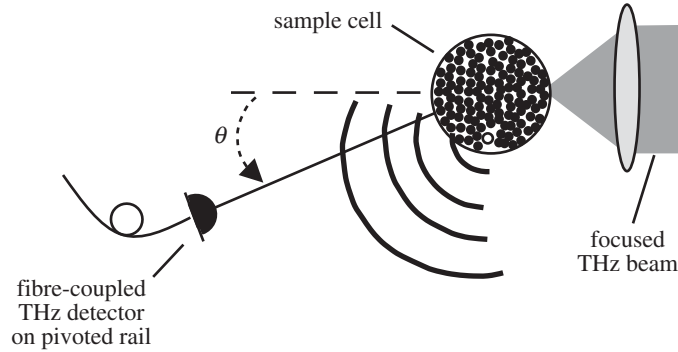


Figure 1. Schematic of the experimental set-up, showing the fibre-coupled THz detector positioned at an angle θ with respect to the transmitted beam. A spherical wave produced by a hypothetical scattering event, centred to the right of the axis of the displayed detector location, is also shown. This partial spherical wave would produce a correlated signal on detectors at different locations, with a temporal shift resulting from the geometrical path length difference. In the case illustrated here, a detector at a larger angle θ would receive the signal earlier.

throughout the spectral range of the measurements (Birch *et al.* 1981). The volume fraction of the spheres in the sample cell is measured to be 0.56 ± 0.04 . Our previous measurements indicate that the mean free path in these samples ranges from *ca.* 1 to *ca.* 70 mm within the bandwidth of the terahertz pulse (Pearce & Mittleman 2001, 2002).

Figure 2 shows several representative terahertz waveforms. Each output waveform corresponds to a realization of a unique configuration of the random medium. These waveforms have been spectrally filtered at both low and high frequencies to improve the signal-to-noise ratio, which is about 10:1 at the spectral peak. For reference, the signal-to-noise ratio for a measurement of the incident single-cycle pulse (figure 2*a*) exceeds 20 000 after equivalent spectral filtering. The result of the multiple scattering is a randomization of the phase, which produces the complex structure shown in figure 2. By taking the Fourier transform of these waveforms, we can extract both the real $r = \text{Re}[E(\omega)]$ and the imaginary $i = \text{Im}[E(\omega)]$ parts of the scattered electric field $E(\omega)$. From these measurements, we are able to obtain the probability distribution of the real and imaginary parts of the transmitted field, $P(r)$ and $P(i)$.

If we assume that the complex electric field component at a given frequency is the sum of a large number of random phasors, then the central limit theorem predicts that the scattered field should obey Gaussian statistics (Chabanov & Genack 1997; Goodman 2000). Assuming that the phase is uniformly distributed, the joint probability distribution of the real and imaginary parts at a given frequency ω can be considered zero-mean jointly Gaussian variables, and therefore

$$P(r, i | \omega) = \frac{1}{2\pi\sigma_\omega(\omega)^2} \exp\left[-\frac{r^2 + i^2}{2\sigma_\omega(\omega)^2}\right] \quad (2.1)$$

where the variance $\sigma_\omega(\omega)^2 = \frac{1}{2}\langle I(\omega) \rangle$. Here, $\langle I(\omega) \rangle$ is the spectral intensity of the diffuse light averaged over all configurations of the medium and it is dependent on the input pulse spectrum and the scattering parameters of the random media. To determine the joint distribution of the real and imaginary parts within a finite frequency range $\Delta\omega = \omega_2 - \omega_1$, we integrate (2.1) over ω and normalize by the

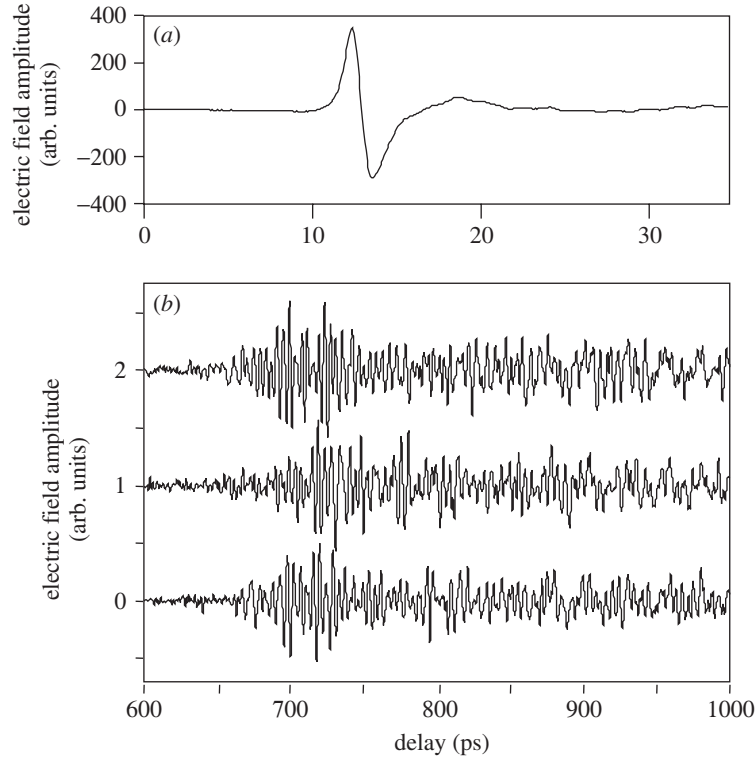


Figure 2. (a) A typical input waveform. (b) Three typical scattered waveforms, for three different configurations of the random medium. These waveforms have been vertically offset, for clarity. In (b), the amplitudes are arbitrary but can be compared with the amplitude of the input waveform shown in (a). The time axis of (b) has an arbitrary origin (see figure 5 and associated discussion).

bandwidth $\Delta\omega$, to get

$$P(r, i) = \frac{1}{\pi\Delta\omega} \int_{\omega_1}^{\omega_2} d\omega \frac{1}{\langle I(\omega) \rangle} \exp\left[-\frac{r^2 + i^2}{\langle I(\omega) \rangle}\right]. \quad (2.2)$$

This expression may be interpreted as the sum of a large number of zero-mean Gaussian distributions (one for each spectral component), each with a unique variance proportional to $\langle I(\omega) \rangle$. The marginals $P(r)$ and $P(i)$ are equivalent to each other and can be computed as

$$P(a) = \frac{1}{\Delta\omega} \int_{\omega_1}^{\omega_2} d\omega \frac{1}{\sqrt{\pi\langle I(\omega) \rangle}} \exp\left[-\frac{a^2}{\langle I(\omega) \rangle}\right], \quad (2.3)$$

with $a = r, i$, and with variance

$$\sigma^2 = \frac{1}{2\Delta\omega} \int_{\omega_1}^{\omega_2} d\omega \langle I(\omega) \rangle.$$

The variance of $P(r, i)$ is proportional to the integrated average intensity of the diffuse light. This is analogous to a monochromatic speckle pattern, where the variance is proportional to the average intensity (Chabanov & Genack 1997).

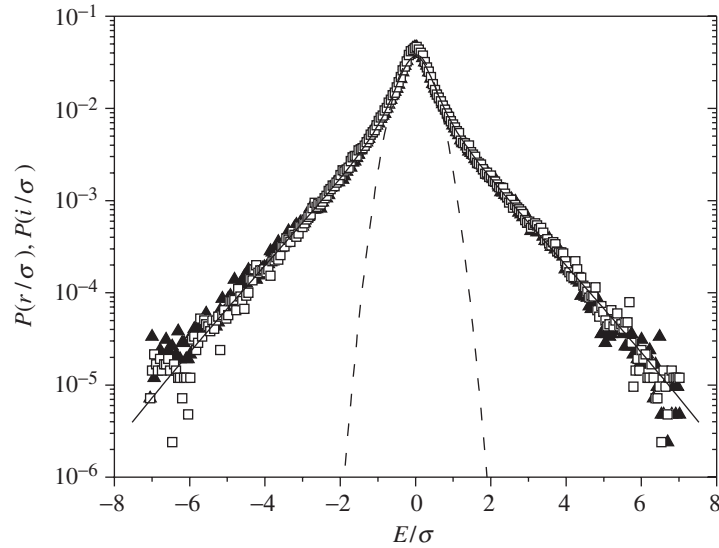


Figure 3. The probability distribution of the normalized real (triangles) and imaginary (open squares) parts of the complex scattered electric field, $P(r/\sigma)$ and $P(i/\sigma)$, plotted on a log scale. The dashed line shows the Gaussian distribution, which is the result expected for monochromatic radiation (Chabanov & Genack 1997). The solid curve is the prediction of equation (2.3), using an experimentally determined estimate for the mean spectral intensity.

We measure waveforms for 22 distinct configurations of the random medium. For each, we extract the complex parts of $E(\omega)$ over the 50–500 GHz spectral range, where there is appreciable signal in the measured waveforms. The probability distributions of the normalized real and imaginary parts $P(r/\sigma)$ and $P(i/\sigma)$ are shown in figure 3. The real and imaginary parts are zero-mean and have nearly identical distributions, as predicted by (2.2). As anticipated, the Gaussian distribution expected for the case of monochromatic illumination (Chabanov & Genack 1997) (dashed line) does not accurately describe the data. In order to compare with the predicted result (equation (2.3)), we extract an estimate of the average intensity $\langle \hat{I}(\omega) \rangle$ by averaging the frequency-dependent intensity spectrum over the 22 measured waveforms. By substituting $\langle \hat{I}(\omega) \rangle$ for the average intensity in (2.3), we can numerically calculate $P(a/\sigma)$. The result (solid line) is in excellent agreement with the experimental data.

The statistics of the phase derivative $d\phi/d\omega \equiv \phi'$ are also of great importance. In the case of narrowband wave packets, the ensemble average of this quantity is inversely proportional to the transport velocity, so it can be interpreted as a time delay for photons in the medium. For broadband waves, its connection to the concept of a delay time is questionable, because of the randomization of the spectral phase. Nevertheless, it is instructive to investigate the statistics of ϕ' , because of its relevance in the study of higher-order (i.e. C_2) correlations (van Tiggelen *et al.* 1999). For narrowband wave packets, the probability distribution for the normalized phase derivative has been derived within the Gaussian approximation as (Genack *et al.* 1999; van Tiggelen *et al.* 1999)

$$P\left(\hat{\phi}' \equiv \frac{\phi'}{\langle \phi' \rangle}\right) = \frac{\frac{1}{2}Q}{[Q + (Q + (\hat{\phi}' - 1))^2]^{3/2}}, \quad (2.4)$$

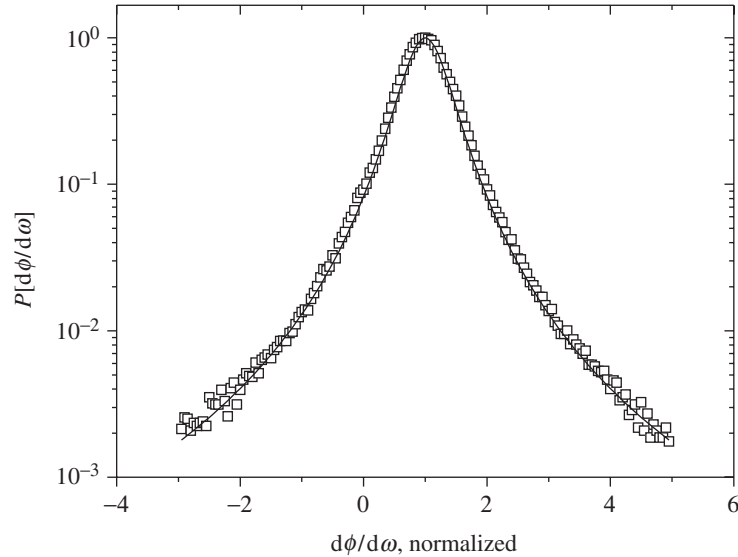


Figure 4. The probability distribution of the normalized spectral phase derivative $\hat{\phi}'$, plotted on a log scale. The solid line is the probability distribution given in (2.4), equivalent to the monochromatic case (van Tiggelen *et al.* 1999), with $Q = 0.234$.

where $\hat{\phi}'$ is the phase derivative normalized to its ensemble-averaged mean and where Q is a parameter related to the absorption length L_a and the sample geometry. We note that this relation between Q and L_a is not trivial to compute except for very simple sample geometries such as the case of normal incidence on a thin slab (Berkovits & Feng 1994).

For broadband waves, $P(\hat{\phi}')$ can be derived by integrating (2.4) over frequency with an appropriate weighting function, as in equations (2.2) and (2.3) above. However, because, in our measurements, the absorption length is approximately constant over the entire bandwidth of the radiation, Q should not vary much as a function of frequency. Since this is the only parameter, the distribution of the phase derivative for broadband waves should also be given by (2.4). Figure 4 shows the probability distribution for $\hat{\phi}'$, extracted from the Fourier transforms of the measured waveforms. The solid curve is the predicted result (equation (2.4)), with $Q = 0.234$. As anticipated, the theoretical expression derived for the monochromatic case can also accurately predict the statistics of the broadband wave packet.

3. Spatiotemporal field correlations

With a good understanding of the statistical nature of the measured fields, we now turn to an investigation of the correlations between fields measured at different spatial locations. In essence, this is a study of speckle patterns, but with a time resolution sufficient to resolve a single cycle of the field. As we shall demonstrate, this measurement permits us to obtain information about the locations of *individual scattering events* experienced by portions of the diffusing field (Jian *et al.* 2003). Such data are typically not experimentally accessible because the measured field generally consists of a superposition of many random phasors, corresponding to waves that have

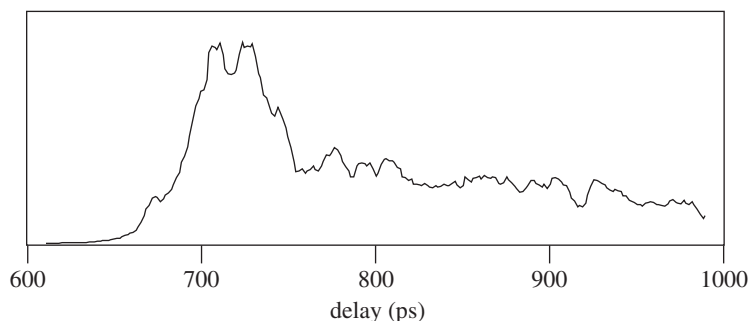


Figure 5. Photon time-of-flight distribution, determined from the data by averaging the squares of the measured waveforms. This serves as a sort of calibration for the delay axis, as described in the text.

traversed many different possible paths (Goodman 2000). However, by computing the temporal correlations between waves measured at different spatial locations, we are able to highlight the portions that originate from a single scattering event. This represents a completely new method for characterizing a random medium, since the concept of locating individual scattering events within a diffusing wave has not previously been considered. We note that it has recently become possible to measure the amplitude and phase of ultra-short optical pulses (Trebino 2002), so our results could, in principle, be extended to biologically relevant wavelengths in the near infrared. Thus these measurements open up new possibilities for imaging in biological media.

The experimental configuration is the same as shown in figure 1. Because the random medium is static, we can measure numerous portions of the scattered field with a single detector, simply by repositioning the detector. For each fixed configuration of the random medium, we measured waveforms at angles within two groups, at $\theta = 65, 66, \dots, 75^\circ$ and $\theta = 105, 106, \dots, 115^\circ$, corresponding to forward and backward scattering, respectively. We note that all of our waveforms, as with most THz TDS experiments, are measured on an arbitrary time axis. That is, the zero of the time axis is arbitrarily specified and is not equal to the time at which the pulse is generated. For this reason, it is difficult to extract absolute photon transit times within the random medium, since we do not have an accurate measurement of the time at which the pulse entered the sample. However, the arbitrary offset is the same for all measurements, so relative delays can still be extracted from these data. In order to provide some sense of the meaning of the time axis, we show in figure 5 a determination of the photon time-of-flight distribution, obtained by averaging the squares $|E(t)|^2$ of all of our measured waveforms. These data can serve as a sort of calibration for the time axis, since they show the time at which the first photons reached the detector after emerging from the sample. All scattered waveforms in this paper (including those shown in figure 2) are plotted on the same time axis used in figure 5.

For a given random configuration, we expect that the correlation between fields measured at two different angles, $\langle E_{\theta_1}(t)E_{\theta_2}(t) \rangle$, decreases with increasing $\delta\theta \equiv \theta_2 - \theta_1$ (Goodman 2000). Since we directly measure $E(t)$, we may easily compute this correlation coefficient, averaged over all configurations for each value of $\delta\theta$. The result, shown in figure 6, exhibits an exponential decay, with an angular $1/e$ width of *ca.* 3.7° . This is essentially a measure of the mean size of a speckle spot, which

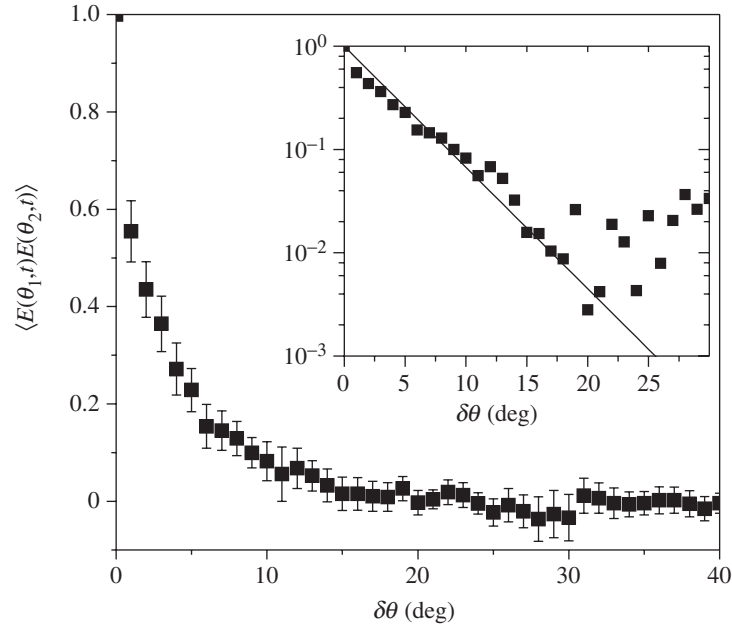


Figure 6. Ensemble-averaged electric-field correlation coefficients at zero offset as a function of the angular separation $\delta\theta$ between the measurement points. The inset shows the data on a log scale, indicating an exponential decay of the spatial correlation, $\exp[-\delta\theta/3.7^\circ]$, to the noise floor at $\delta\theta \sim 18^\circ$.

is related to the illuminated area on the sample cell input facet (Berkovits & Feng 1990; Tomita & Matsuoka 1991).

A more surprising result can be found by computing the correlation function between portions of the measured time-domain waveforms, rather than using the entire waveform. By choosing a temporal window, one can highlight correlations that occur at particular time delays. For example, we expect that the later parts of a particular pair of waveforms show smaller correlations than the earlier parts, since these late-arriving parts have scattered more times (Snieder *et al.* 2002). In addition, partial waves may arrive at each detector location with a different delay, so correlated signals may appear at non-zero values of the correlation offset. To formalize the computational procedure, we define a correlation function with a variable-delay window,

$$C_{\delta\theta}(\tau, T) = \frac{1}{C_0} \langle [E_{\theta_1}(t) \cdot W_T(t)][E_{\theta_2}(t + \tau) \cdot W_T(t + \tau)] \rangle,$$

where τ is the correlation offset and $W_T(t)$ is a window function centred at $t = T$, defined to be unity in a symmetric window about $t = T$ and zero otherwise. The window width is fixed at 50 ps, approximately equal to the inverse coherence bandwidth for our experimental geometry (Ishimaru 1978). As usual, the angular brackets indicate integration with respect to t , followed by an ensemble average over all waveform pairs with the specified value of $\delta\theta$. C_0 is a normalization factor, which ensures that $C_{\delta\theta=0}(\tau = 0, T) = 1$. This windowed correlation function is similar to the one recently used for the analysis of coda waves in seismic tomography (Snieder *et al.* 2002).

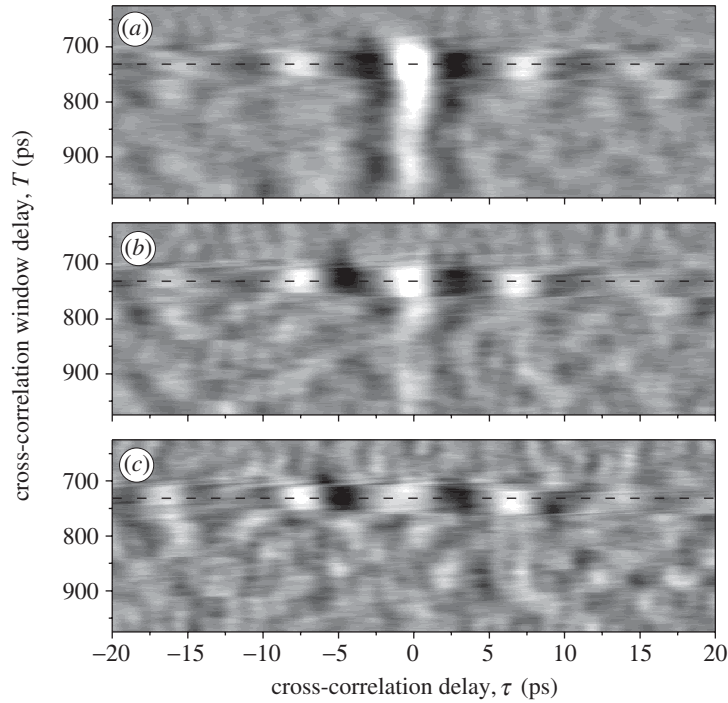


Figure 7. Correlation function $C_{\delta\theta}(\tau, T)$ plotted versus the correlation offset τ and the delay of the temporal window T . The T -axes (vertical axes) are the same as the time axis in figure 5. These data represent an ensemble average of all pairs of measured fields with the indicated angular separation, for one particular realization of the random configuration of scatterers. In this example, an extended oscillatory correlation is observed at a window delay of $T \sim 730$ ps. This correlation persists even for large angular separations. The dashed lines indicate cuts through these datasets displayed in figure 8. (a) $\delta\theta = 2^\circ$. (b) $\delta\theta = 5^\circ$. (c) $\delta\theta = 8^\circ$.

A typical result for $C_{\delta\theta}(\tau, T)$ is shown in figure 7, for three different values of $\delta\theta$. Clearly, the correlation at zero offset ($\tau = 0$) decreases with increasing window delay T , as a result of the increasing average number of scattering events. Also, as expected from figure 6, the correlation between pairs of waveforms with $\delta\theta = 8^\circ$ is nearly zero, since this is more than twice the angular speckle decay width. However, a strong oscillatory signal, indicating a correlation extending over several cycles of the field, is observed at window delay of $T \sim 730$ ps. This extended correlation is observed at this value of T for many angular separations, even those which are larger than the angular width of a typical speckle spot. This surprising feature arises when a partial wave from *one particular scattering event* gives rise to synchronized (though not simultaneous) signals at all detector locations. In the example shown here, only one scattering event is observed. However, for other configurations of the random medium, we generally observe numerous oscillatory signatures, occurring at various values of T .

From $C_{\delta\theta}(\tau, T)$, it should be possible to determine the location of the particular scattering event that gave rise to the observed correlation. Here, we use the evolution of the phase of the correlation to determine the direction from the detector to the scattering event. As shown in figure 8, this phase evolves in a systematic way with

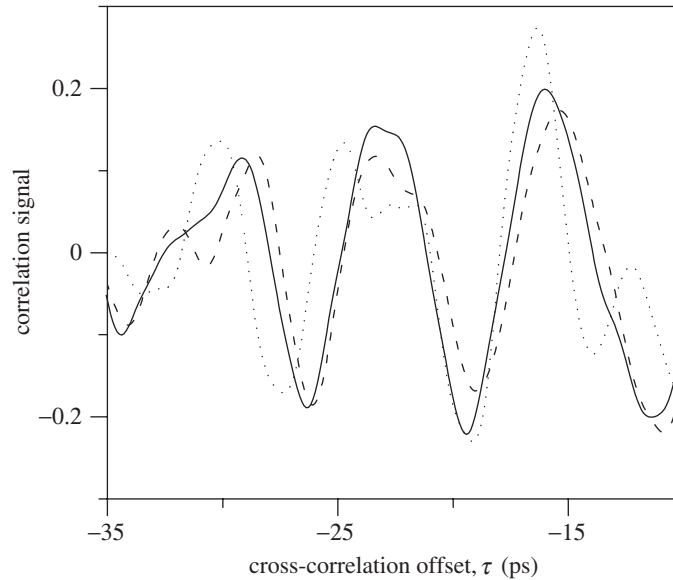


Figure 8. Three cuts through the data of figure 7, along the horizontal dashed lines in each of the three panels. These show the evolution of a portion of the oscillatory correlation with increasing angular separation (dashed, $\delta\theta = 2^\circ$; solid, $\delta\theta = 5^\circ$; dotted, $\delta\theta = 8^\circ$). As $\delta\theta$ increases, the correlation signal shifts towards negative offsets. This shift is related to the tilt of the correlated wavefront emerging from the random medium. From the rate of the phase shift with increasing $\delta\theta$, it is possible to determine the direction from which the scattered signal emerged.

increasing $\delta\theta$. In these data, the oscillations shift to larger negative correlation offset with increasing $\delta\theta$. This indicates that, for waveforms with larger angular separation, a larger (negative) temporal offset is required to cause the oscillations in one waveform to coincide with those in the other. This offset is a result of the geometrical path length difference arising from the tilt of the wavefront. This increasing *negative* shift with increasing $\delta\theta$ means that the correlated portion of the wavefront arrived earlier at detectors with larger values of θ , and therefore the corresponding scattering event took place on the side of the detector axis closer to the sample input facet. Conversely, an increasing *positive* shift with increasing $\delta\theta$ would be observed if the scattering event took place on the opposite side of the detector axis from the input facet. Thus the evolution of the correlation phase is a direct indication of the direction of the scattering event relative to the detector axis.

From numerous measurements of the type illustrated in figure 8, we can collect statistics on the value of the correlation phase shift. This gives a direct measurement of the degree of asymmetry of the radiation emerging from the random medium. We have measured both forward and backward scattering for four distinct configurations of the random medium. We have computed $C_{\delta\theta}(\tau, T)$ for these eight cases and have tabulated the parameters of the numerous oscillatory correlation signatures in each. In these eight datasets, we have observed a total of 98 such signatures, each corresponding to a unique scattering event. For each of these, we have extracted a numerical value for the phase shift of the oscillatory component, as described above. These 98 results are displayed in figure 9, divided according to whether the signal was extracted from the forward or backward scattering datasets.

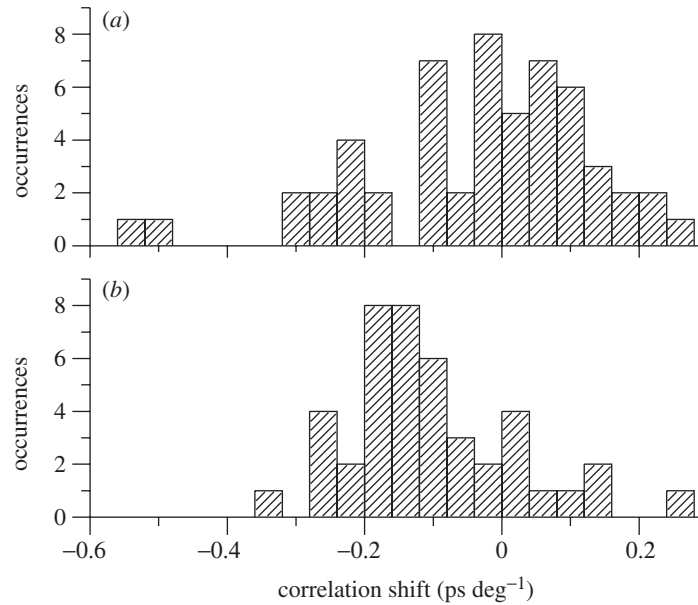


Figure 9. Histograms of the correlation phase shift, for all of the observed scattering events in measurements of four distinct random configurations. These are displayed for both the case of forward ($\theta = 65, \dots, 75^\circ$) and backward ($\theta = 105, \dots, 115^\circ$) scattering. The forward-scattering events exhibit an asymmetric correlation phase, indicating that the scattering events are more likely to originate from the side of the detector axis closer to the input beam. In contrast, the backward-scattering events are nearly symmetric. (a) $\theta = 110^\circ \pm 5^\circ$. (b) $\theta = 70^\circ \pm 5^\circ$.

These histograms represent a compelling illustration of the new information that can be obtained using our approach. We have determined that, in the backward direction, the scattering events are largely symmetric. That is, a detector in this region is equally likely to detect scattering events located to the left and right of the detector axis. This follows from the fact that the mean value of the correlation phase shift is approximately zero ($-0.03 \pm 0.04 \text{ ps deg}^{-1}$). On the other hand, in the forward direction, the mean value is negative ($-0.10 \pm 0.04 \text{ ps deg}^{-1}$). This indicates a marked asymmetry, with more scattering events located on the side of the detector closer to the input facet.

4. Conclusion

We report the first use of THz TDS in the study of diffuse waves. The direct measurement of the multiply scattered electric field allows for the computation of statistics for both amplitude and phase. We have extended the theoretical framework, developed for monochromatic waves, to the broadband case, and found excellent agreement with our measured results. In addition, we have demonstrated a unique method for characterizing the diffusive radiation emerging from a random medium, involving the measurement of both its amplitude and phase. We have developed a simple computational tool that highlights the correlations buried within these random waveforms. Using this technique, it is possible to extract information about specific scattering events, which is not possible using conventional measurements. This work should

spur further theoretical considerations, since the possibility of time-resolved field measurements has not been considered, other than in a waveguide geometry where imaging considerations are not relevant. Also, we expect that analogous information could be obtained using near-infrared or visible light diffusing through biological tissue. This could, in turn, lead to a new method for diffuse photon imaging with phase coherent detection.

This work has been supported in part by the US National Science Foundation.

References

- Bashkansky, M., Adler, C. L. & Reintjes, J. 1994 Coherently amplified Raman polarization gate for imaging through scattering media. *Opt. Lett.* **19**, 350–352.
- Berkovits, R. & Feng, S. 1990 Theory of speckle-pattern tomography in multiple-scattering media. *Phys. Rev. Lett.* **65**, 3120–3123.
- Berkovits, R. & Feng, S. 1994 Correlations in coherent multiple scattering. *Phys. Rep.* **238**, 135–172.
- Birch, J. R., Dromey, J. D. & Lesurf, J. 1981 The optical constants of some common low-loss polymers between 4 and 40 cm^{-1} . *Infrared Phys.* **21**, 225–228.
- Boas, D. A. & Yodh, A. G. 1997 Spatially varying dynamical properties of turbid media probed with diffusing temporal light correlation. *J. Opt. Soc. Am. A* **14**, 192–215.
- Boas, D. A., Campbell, L. E. & Yodh, A. G. 1995 Scattering and imaging with diffusing temporal field correlations. *Phys. Rev. Lett.* **75**, 1855–1858.
- Brodsky, A., Shelley, P. H., Thurber, S. R. & Burgess, L. W. 1997 Low-coherence interferometry of particles distributed in a dielectric matrix. *J. Opt. Soc. Am. A* **14**, 2263–2268.
- Brodsky, A., Thurber, S. R. & Burgess, L. W. 2000 Low-coherence interferometry in random media. I. Theory. *J. Opt. Soc. Am. A* **17**, 2024–2033.
- Chabanov, A. A. & Genack, A. Z. 1997 Field distributions in the crossover from ballistic to diffusive wave propagation. *Phys. Rev. E* **56**, R1338–R1341.
- Feng, S., Kane, C., Lee, P. A. & Stone, A. D. 1988 Correlations and fluctuations of coherent wave transmission through disordered media. *Phys. Rev. Lett.* **61**, 834–837.
- Genack, A. Z., Garcia, N. & Polkosnik, W. 1990 Long-range intensity correlation in random media. *Phys. Rev. Lett.* **65**, 2129–2132.
- Genack, A. Z., Sebbah, P., Stoytchev, M. & van Tiggelen, B. A. 1999 Statistics of wave dynamics in random media. *Phys. Rev. Lett.* **82**, 715–718.
- Goodman, J. W. 2000 *Statistical optics*. Wiley.
- Herrmann, M., Tani, M., Watanabe, M. & Sakai, K. 2002 Terahertz imaging of objects in powders. *IEE Proc. Optoelectron.* **149**, 116–120.
- Ishimaru, A. 1978 *Wave propagation and scattering in random media*. Academic.
- Jian, Z., Pearce, J. & Mittleman, D. 2003 Characterizing individual scattering events by measuring the amplitude and phase of the electric field diffusing through a random medium. *Phys. Rev. Lett.* **91**, 033903.
- Lasocki, D. L., Matson, C. L. & Collins, P. J. 1998 Analysis of forward scattering of diffuse photon-density waves in turbid media: a diffraction tomography approach to an analytic solution. *Opt. Lett.* **23**, 558–560.
- Matson, C. L. 1997 A diffraction tomographic model of the forward problem using diffuse photon density waves. *Opt. Express* **1**, 6–11.
- Mittleman, D. M., Jacobsen, R. H. & Nuss, M. C. 1996 T-ray imaging. *IEEE J. Select. Topics Quant. Electron.* **2**, 679–692.
- Mittleman, D. M., Gupta, M., Neelamani, R., Baraniuk, R. G., Rudd, J. V. & Koch, M. 1999 Recent advances in terahertz imaging. *Appl. Phys. B* **68**, 1085–1094.

- Naulleau, P., Dilworth, D., Leath, E. & Lopez, J. 1995 Detection of moving objects embedded within scattering media by use of speckle methods. *Opt. Lett.* **20**, 498–500.
- O’Leary, M. A., Boas, D. A., Chance, B. & Yodh, A. G. 1992 Refraction of diffuse photon density waves. *Phys. Rev. Lett.* **69**, 2658–2661.
- O’Leary, M. A., Boas, D. A., Chance, B. & Yodh, A. G. 1995 Experimental images of heterogeneous turbid media by frequency-domain diffusing-photon tomography. *Opt. Lett.* **20**, 426–428.
- Pearce, J. & Mittleman, D. M. 2001 Propagation of single-cycle terahertz pulses in random media. *Opt. Lett.* **26**, 2002–2004.
- Pearce, J. & Mittleman, D. M. 2002 Scale model experimentation: using terahertz pulse to study light scattering. *Phys. Med. Biol.* **47**, 3823–3830.
- Pearce, J., Jian, Z. & Mittleman, D. 2003 Statistics of multiply scattered broadband terahertz pulses. *Phys. Rev. Lett.* **91**, 043903.
- Petoukhova, A. L., Steenbergen, W. & de Mul, F. F. M. 2001 Path-length distribution and path-length-resolved Doppler measurements of multiply scattered photons by use of low-coherence interferometry. *Opt. Lett.* **26**, 1492–1494.
- Pine, D. J., Weitz, D. A., Chaikin, P. M. & Herbolzheimer, E. 1988 Diffusing-wave spectroscopy. *Phys. Rev. Lett.* **60**, 1134–1137.
- Popescu, G. & Dogariu, A. 1999 Optical path-length spectroscopy of wave propagation in random media. *Opt. Lett.* **24**, 442–444.
- Ripoll, J. & Nieto-Vesperinas, M. 1999 Reflection and transmission coefficients for diffuse photon density waves. *Opt. Lett.* **24**, 796–798.
- Rivas, J. G., Sprik, R. & Lagendijk, A. 2001 Static and dynamic transport of light close to the Anderson localization transition. *Phys. Rev. E* **63**, 46 613.
- Schotland, J. C. & Markel, V. A. 2001 Inverse scattering with diffusing waves. *J. Opt. Soc. Am. A* **18**, 2767–2777.
- Sebbah, P., Pnini, R. & Genack, A. Z. 2000 Field and intensity correlation in random media. *Phys. Rev. E* **62**, 7348–7352.
- Snieder, R., Grêt, A., Douma, H. & Scales, J. 2002 Coda wave interferometry for estimating nonlinear behavior in seismic velocity. *Science* **295**, 2253–2255.
- Thompson, C. A., Webb, K. J. & Weiner, A. M. 1997 Imaging in scattering media by use of laser speckle. *J. Opt. Soc. Am. A* **14**, 2269–2277.
- Thurber, S. R., Burgess, L. W., Brodsky, A. & Shelley, P. H. 2000 Low-coherence interferometry in random media. II. Experiment. *J. Opt. Soc. Am. A* **17**, 2034–2039.
- Tomita, M. & Matsuoka, M. 1991 Temporal fluctuations in disordered static optical media. *Phys. Rev. B* **43**, 13 579–13 582.
- Trebino, R. 2002 *Frequency-resolved optical gating: the measurement of ultrashort laser pulses*. Dordrecht: Kluwer Academic.
- van Tiggelen, B. A., Sebbah, P., Stoytchev, M. & Genack, A. Z. 1999 Delay-time statistics for diffuse waves. *Phys. Rev. E* **59**, 7166–7172.
- Webster, M. A., Webb, K. J. & Weiner, A. M. 2002 Temporal response of a random medium from third-order laser speckle frequency correlations. *Phys. Rev. Lett.* **88**, 033901.
- Yoo, K. M., Xing, Q. & Alfano, R. R. 1991 Imaging objects hidden in highly scattering media using femtosecond second-harmonic-generation cross-correlation time gating. *Opt. Lett.* **16**, 1019–1021.
- Yoo, K. M., Das, B. B. & Alfano, R. R. 1992 Imaging of a translucent object hidden in a highly scattering medium from the early portion of the diffuse component of a transmitted ultrafast laser pulse. *Opt. Lett.* **17**, 958–960.

Discussion

P. PLANKEN (*University of Technology Delft, The Netherlands*). There must be some mathematical definition of what randomness really is, and how you decide that your

sample is really a random medium. Is it possible that there is some long-range order, for example, near the windows where all the spheres must be pressed?

D. M. MITTLEMAN. That is an excellent question and it is something that people fight about all the time! There is an extensive literature going back fifty years and you find that if you pour spheres into a box, there is a correlation function that provides a really good description except within two or three diameters of any edge; near edges, the problem becomes much more complicated. The correlation function describes exactly the positional correlations and tells you if there is a sphere here, how likely that there is a sphere anywhere else. And even at these high densities, you see four or five oscillations in this correlation function before it stops oscillating and at that point there is no longer any correlation. So you can be pretty confident that there are no long-range correlations, but on a length-scale of five diameters or so from any sphere there is definitely correlation and you have to take that into account. The other solution, and one of the next experiments that we are going to do, is to look at higher index random media comprising randomly shaped grains. In this case, you do not have to worry about it nearly as much; if the poly-dispersity is more than about 10%, you just get one oscillation and it stops. You only get these correlation effects if you are using scatterers which are all of the same size and shape.

K. UNTERRAINER (*Institute of Solid-State Electronics, Vienna University of Technology, Austria*). I see no reflections from the windows in your ballistic measurements.

D. M. MITTLEMAN. The average index of the spheres in air is 1.25 or 1.26 and the index of the window is about 1.42, so that is not a very big difference. So, on the inner surfaces, the reflection is very small. On the outer surfaces you are going to get a reflection, but it falls late enough in time that you can time gate it away. But, yes, you certainly have to think about that.